inorganics

MDPI

Review

Atomic Layer Deposition on Porous Materials: Problems with Conventional Approaches to Catalyst and Fuel Cell Electrode Preparation

Tzia Ming Onn [1], Rainer Küngas [2], Paolo Fornasiero [3], Kevin Huang [4] and Raymond J. Gorte [1,*]

1 Department of Chemical and Biomolecular Engineering, University of Pennsylvania, 34th Street, Philadelphia, PA 19104, USA; tonn@seas.upenn.edu
2 Haldor Topsöe A/S, Haldor Topsøes Allé 1, 2800 Kongens Lyngby, Denmark; rainerkungas@gmail.com
3 Department of Chemical and Pharmaceutical Sciences, ICCOM-CNR, Consortium INSTM, University of Trieste, via L. Giorgieri 1, 34127 Trieste, Italy; pfornasiero@units.it
4 Department of Mechanical Engineering, University of South Carolina, Columbia, SC 29201, USA; HUANG46@cec.sc.edu
* Correspondence: gorte@seas.upenn.edu

Received: 12 February 2018; Accepted: 10 March 2018; Published: 13 March 2018

Abstract: Atomic layer deposition (ALD) offers exciting possibilities for controlling the structure and composition of surfaces on the atomic scale in heterogeneous catalysts and solid oxide fuel cell (SOFC) electrodes. However, while ALD procedures and equipment are well developed for applications involving flat surfaces, the conditions required for ALD in porous materials with a large surface area need to be very different. The materials (e.g., rare earths and other functional oxides) that are of interest for catalytic applications will also be different. For flat surfaces, rapid cycling, enabled by high carrier-gas flow rates, is necessary in order to rapidly grow thicker films. By contrast, ALD films in porous materials rarely need to be more than 1 nm thick. The elimination of diffusion gradients, efficient use of precursors, and ligand removal with less reactive precursors are the major factors that need to be controlled. In this review, criteria will be outlined for the successful use of ALD in porous materials. Examples of opportunities for using ALD to modify heterogeneous catalysts and SOFC electrodes will be given.

Keywords: atomic layer deposition; heterogeneous catalysts; SOFC; thin films; diffusion limitations; vapor-solid reaction; ceria; perovskites

1. Introduction

1.1. Opportunities for Using ALD

It has been estimated that 35% of the global economy is dependent, either directly or indirectly, on processes that use heterogeneous catalysts [1]. Since the reaction rates and selectivities over a given catalyst can dramatically affect the economics and energy efficiency of the catalytic process, there has been a continuing research effort over the years to come up with increasingly better materials. For many processes, the catalysts are multicomponent, consisting of catalytically active components and promoters, and are usually deposited onto a support material that provides high surface areas. The catalytically active component may consist of more than one element, as in the case of alloys; the support material may itself be a catalyst or a promoter, such as in the case of ceria–zirconia in automotive three-way catalysts [2–5]. For a number of reactions, the catalytically active sites may exist at the points of contact between the various components that make up the material [6–8]. Since catalytic reactions occur on the molecular scale, this implies that the materials must be engineered on the atomic scale.

Solid oxide fuel cells are unmatched in their efficiency when converting chemical energy to electrical energy; however, improvements in the performance and stability of the electrodes are still required for commercial viability. Interestingly, there are many similarities between SOFC (solid oxide fuel cell) electrodes and some heterogeneous catalysts. SOFC electrodes must be porous and are usually composites, with different components acting as catalysts or as ionic and electronic conductors. Since the electrochemical reactions occur at three phase boundary (TPB) sites, which are defined as the sites where the gas phase, the electronic conductor, and the electrolyte all come together, structure is critically important [9]. The electronically conductive phase of the electrode is often also catalytic, but this is not always true. Examples exist where the addition of a separate catalytic phase can greatly improve performance [10–13]. There can also be advantages to coating one of the phases in the electrode. For example, it has been shown that films of CeO_2 or BaO [14,15] on the Ni in some SOFC anodes can lead to improved tolerance to coking. Similar to the case for heterogeneous catalysts, engineering the structure of the electrode on an atomic scale can be very important.

While scientists have been very successful in developing effective heterogeneous catalysts and SOFC electrodes, recent developments in nanotechnology have greatly expanded our ability to control the synthesis of the active sites for these applications. Among the most interesting nanotechnology tools for this purpose is atomic layer deposition. In ALD, the surface that is being modified is first allowed to react with a molecular precursor, after which the ligands of the adsorbed molecular precursor are removed in a separate step. Since the ligands from the adsorbed precursors prevent additional reactions, film growth is limited to no more than one monolayer in this cycle. However, the cycle of precursor exposure and reaction can be repeated to grow films of any desired thickness. Precursor molecules are available for much of the periodic table [16]; and the deposition of pure oxides, nitrides, sulfides, and mixed oxides has been demonstrated. Overall, the layer-by-layer nature of ALD gives unprecedented control in synthesizing materials with well-defined composition and structure [17].

1.2. Problems with Conventional ALD Approaches to Catalyst and Electrode Preparation

The potential of ALD to prepare novel catalysts and SOFC electrodes is well recognized, and a number of excellent reviews are available for both types of materials [18–27]. However, much of the past ALD work on preparing catalysts and SOFC electrodes has used equipment and procedures that have been developed by the semiconductor industry for deposition on relatively flat surfaces, rather than highly porous surfaces. A careful survey of this literature demonstrates that using conventional ALD approaches can lead to serious problems when applied to catalyst and electrode synthesis. It also greatly limits the potential applications of ALD, as well as the benefits that can be derived from using ALD to prepare materials.

The first problem is that film growth rates on porous materials are often reported to be unrealistically high or low. While growth rates will depend on the precursor and surface, these are typically reported to be between 0.01 and 0.1 nm/cycle, values that correspond well to that which would be calculated based on the thickness of a precursor monolayer [28]. In apparent contradiction with this, two groups have reported growing ZrO_2 films in porous SOFC electrodes at rates between 0.5 and 0.6 nm/cycle [29,30]. Another group reported growing metallic W films at 0.4 nm/cycle, although the diameter of a W atom is only 0.25 nm [31]. Still, other groups have reported results that would indicate very low growth rates. One ALD study of MnO on 200-m^2/g SiO_2 achieved an Mn loading of 0.33 wt % after five ALD cycles [32], even though the reported growth rate of 0.08 nm/cycle for the precursor that was used should have given an MnO loading nearly 100 times that value for uniform film growth [33]. In another example, 75 ALD cycles of Fe_2O_3 on 40-m^2/g Al_2O_3 achieved a loading of only 1.1 wt %, which corresponds to a growth rate of only 0.0007 nm/cycle if the film grew uniformly over the surface [34,35].

A second major problem involves the cost of the precursors. In a conventional ALD system that employs a carrier gas to introduce the precursor to the substrate, a significant fraction of the precursor will exit the system with the carrier. For high-value semiconductor devices, this may be acceptable, so

long as the precursors are not too expensive. For catalyst and SOFC applications, this cost will likely be prohibitive.

Finally, conventional ALD procedures limit the choice of precursors that one can use. The temperature window for ALD is relatively narrow, since temperatures must be high enough for the precursor to react with the surface, and low enough to avoid chemical vapor deposition. For many potentially interesting precursors, the ligands cannot be easily removed in this temperature range. An example of this occurred with the precursor used in a recent study to deposit La_2O_3, $La(TMHD)_3$ (Tris(2,2,6,6-tetramethyl-3,5-heptanedionato) lanthanum) [36–38]. The organic ligands on this molecule are not removed by water or O_2 at ALD conditions, and are oxidized by ozone only very slowly.

In the next sections, we will address these issues and show that many of these issues can be solved by changing the procedures that are used to perform ALD.

1.3. Design Considerations for Semiconductor Applications

For semiconductor applications, films are grown on relatively flat surfaces where diffusion of the precursor molecules onto the surface is rapid. In some cases, there may be channels into the surface, but the aspect ratio of these channels—the ratio of the channel depth to width—is rarely greater than 100 [39,40]. The desired films are also reasonably thick, usually greater than 2 nm and often up to 20 nm [39,40]. For an ALD film growth rate of 0.04 nm/cycle, even a 2-nm film would require 50 cycles, whereas a 20-nm film would require 500 cycles. Each cycle involves at least four separate steps: (1) exposure to the precursor; (2) purge the excess precursor; (3) exposure of reagent to remove ligands (e.g., exposure to an oxidizer to form an oxide); and (4) purge the ligand removal reagent prior to precursor exposure.

To make this process cost effective, conventional ALD equipment is designed to do each step as rapidly as possible. This is accomplished most commonly by using a flow reactor, with the precursors and ligand-removal reagents being transported into and out of the deposition chamber via a carrier gas that is also used for the purge steps (Figure 1). The flow rates of the carrier gas are typically in the order of 100 mL/min to 200 mL/min, corresponding to linear gas velocities of 2.5 m/s to 10 m/s across the substrate [41,42]. The precursor and ligand-removal reagents can be inserted into the carrier stream as short pulses typically of 0.5-s duration [39], and passed over the sample by convection. Due to the high flow velocities, back mixing is negligible.

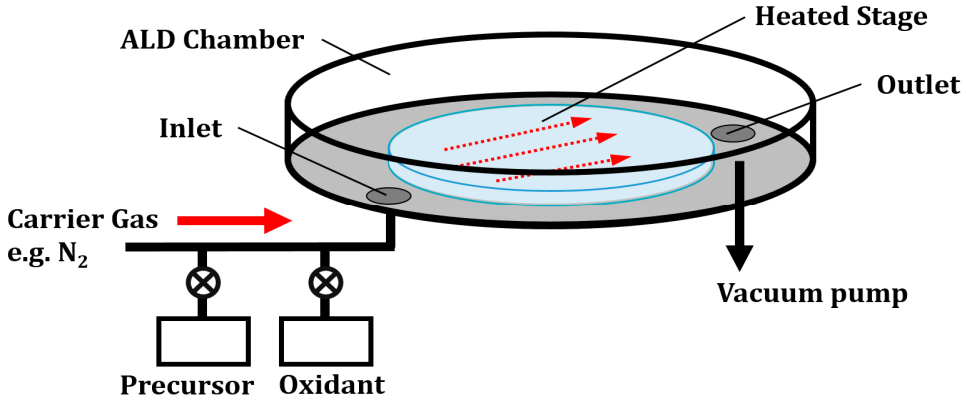

Figure 1. Simplified schematic of a typical research-grade viscous flow atomic layer deposition (ALD) reactor designed for coating flat samples (e.g., Si wafers). The red arrows indicate the direction of gas flow across the sample.

While this design allows rapid cycling, it has serious limitations for porous materials. First, there can be diffusion limitations in high-aspect-ratio pore structures. Diffusion of the precursor and ligand-removal reagents into and out of long pores will be slow and can lead to gradients in the deposition, even when surface reactions are rapid [43,44]. Second, most of the reagents pass through

the reactor without being incorporated into the sample. This is essential for maintaining uniform growth rates along the length of the sample. Recycling the reagents from the carrier stream is usually not practical, since they will have been mixed with the ligand-removal reagent at the reactor exit. For high-value semiconductor devices, the cost of the precursor molecules may not be a critical issue.

1.4. Design Considerations for Catalysts and SOFC Electrodes

The situation for porous materials, such as heterogeneous catalysts and SOFC electrodes, is very different. First, the number of ALD cycles required for sample preparation will be much lower on these high-surface-area materials, making rapid cycling much less important. In some cases, such as the addition of a transition metal to a support or deposition of an overcoating oxide layer to enhance stability [45–47], a few cycles may be sufficient to reach the desired loading. Only rarely will the application require the deposition of a film more than 1 nm thick. For example, consider a typical catalyst support with a surface area of 200 m^2/g. A simple calculation shows that a dense, 1 nm conformal film of a material with a density of 5 g/cm^3 (e.g., Fe_2O_3 has a density of 5.24 g/cm^3) would double the sample weight and have a loading of 50 wt % of the added material. Furthermore, even if the added material did not substantially affect the pore sizes, the surface area per gram would decrease by half.

Second, in catalyst and SOFC electrode applications, it is important not to lose significant amounts of the precursor. This becomes obvious from the above calculation of film weight loading. If half of the catalyst mass consists of the added material, the cost of that material will be a significant fraction of the total catalyst cost. Since the main cost of many precursor molecules results from the high cost of the organic ligands, it is necessary to make full use of the precursor in the sample itself.

Third, diffusional limitations become very important for high-surface-area materials, because the aspect ratio of pores is significantly larger than that found with even the deepest channels in semiconductor devices. For example, even a thin catalyst bed would likely be 100 μm thick and have pores that are 50 nm in diameter, resulting in an aspect ratio of 2000. Industrial catalysts often come in the form of pellets or extrudates that are at least several millimeters in diameter, and can include pores and channels ranging from the macroscale to the nanoscale. Therefore, aspect ratios in industrial catalysts can reach values substantially higher than 2000 [48]. The aspect ratio for SOFC electrodes would be somewhat less, but still very high. To avoid diffusion limitations in powders, it is common to perform the deposition in a rotating or fluidized bed [44,49]. Precursor utilization must be seriously considered in fluidized bed reactors [50], and neither fluidized nor rotating beds can be applied to coating SOFC electrodes. Furthermore, while deposition in agitated beds works well for modifying dense powders, there still can be diffusion limitations within the powder if that powder is porous [51].

In order to design a better system for performing ALD on catalysts and SOFC electrodes, it is important to consider the individual steps in ALD more closely. These will now be considered.

2. Considerations for Performing ALD in Catalysts and SOFC Electrodes

As discussed earlier, a complete ALD cycle consists of four distinct steps: (1) adsorption of the gaseous precursor onto the surface of the substrate; (2) purging the excess precursor and its byproducts from the sample; (3) introduction of a gaseous reactant to remove ligands and regenerate sites; and (4) purging out the excess reactants and their byproducts. These steps are illustrated in Figure 2, and are most thoroughly documented for the Al_2O_3 ALD system, using trimethylaluminum (TMA) as the precursor and water vapor as the reagent for removing the ligands [16,52]. The TMA–water process is close to being ideal for ALD, since the surface reactions shown in Figure 2 are truly self-terminating, both TMA and water are highly reactive, both TMA and water have high vapor pressures at deposition conditions (i.e., there is little tendency for them to form physisorbed, condensed films on the surface), and the gaseous reaction product (methane) is inert [16]. Other ALD systems rely on different precursor chemistries, with some commonly used ligands being halides, alkoxides, β-diketonates, alkyls, and cyclopentadienyls [16,53]. In many cases, the precursors are allowed to react with the surfaces at

temperatures only modestly above that at which the precursors can condense. While the precise reaction mechanisms are specific to the choice of reactants and the properties of the material to be coated, the general principles governing the deposition are often very similar [16,51].

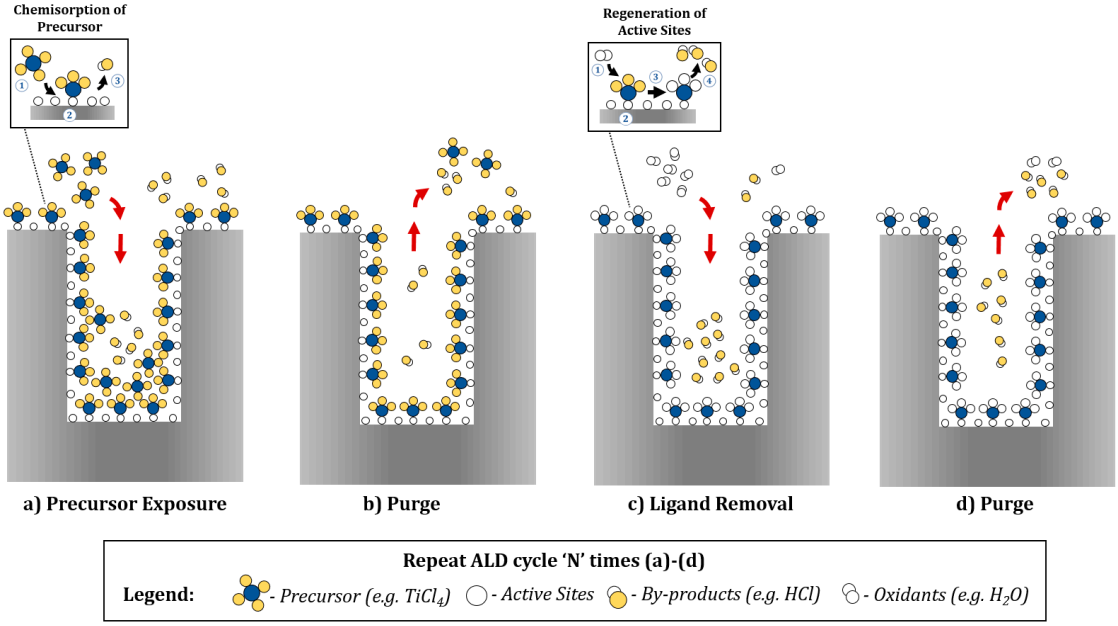

Figure 2. Schematic of one ALD cycle in a pore structure. (**a**) Introduction of precursor molecules and adsorption on the surface; (**b**) purge of the unreacted precursor molecules and reaction products; (**c**) introduction of ligand removal reactants, which react with the chemisorbed precursor molecules; and (**d**) purge of the excess reactants and reaction products. This schematic is an example of an ideal ALD process for TiO_2 deposition using the $TiCl_4/H_2O$ system.

2.1. Adsorption of the Gaseous Precursor onto the Surface of the Substrate

The first step, the exposure of the vapor-phase precursor to the surface of the substrate, requires that the precursor molecules adsorb onto the substrate. Although the adsorption step preferably involves the loss of a ligand and the formation of a chemical bond, physically adsorbed species may be acceptable for some ALD systems on flat surfaces, so long as the single-layer physisorbed species interacts with the surface more strongly than the precursor molecules interact with a condensed film [54]. The advantage to using a physisorbed species is that the coverage of adsorbed precursors will be higher, leading to a higher growth rate [54]. For example, Keuter et al. accurately calculated an expected growth rate for ZrO_2 using tetrakis(ethylmethylamino)-zirconium as the precursor based strictly on the physical size of the molecule, and the calculated surface coverage based on that size [28]. One would expect the density of binding sites for chemisorption to be lower. Uniformity based on physisorbed precursors may be achieved using a flow ALD reactor system on flat samples with short times between pulses; however, for ALD on porous materials, the similarities in the conditions leading to physisorbed monolayers and multilayers will likely lead to variations in the growth rates in different parts of the sample.

When ALD is carried out on flat substrates, such as silicon wafers, the use of a carrier gas increases the rate of mass transport of precursors and reactants from the gas stream onto the substrate surface. This also shortens the length of the required purge step between exposures, leading to shorter ALD cycle times [21]. Flow systems also work reasonably well for coating high-aspect ratio structures with straight pores, and uniform films have been successfully demonstrated on the surface of trenches with aspect ratios of ~100 etched into silicon [55]. However, the use of a carrier gas poses a serious problem when performing ALD on high-surface-area materials. The rapid convective transport of precursors

in the carrier gas flow will not change the diffusion of species into the porous samples. This leads to several problems.

First, the outermost surface of the sample bed will be exposed to precursor fluxes that are several orders of magnitude larger than interior surfaces [22]. The precursor molecules have to diffuse past the already-saturated part near the top of the pores before they can reach the unsaturated, deeper parts of the sample. The diffusion of the precursor into the pores could also be hindered by the counter-diffusion of the carrier gas and the presence of products formed by chemisorption. In order to achieve precursor penetration throughout the high-surface-area material, longer exposure times or multiple exposures are necessary. In one study, precursor exposure times of almost 2 h were required to saturate just 0.2 grams of SiO_2 powder with a specific surface area of 506 m^2/g in a fixed-bed reactor. The entire ALD cycle (consisting of the precursor exposure step, the first purge step, the oxidant exposure step, and the second purge step) lasted 8 h [56].

So long as the mean free path for collisions in the gas phase is shorter than the pore dimensions of the substrate (the typical case for a high-surface-area substrate), the diffusion of precursor molecules into the bed of particles will be the same for a flow system as for a static system. The static system with the adsorption of the precursor onto an evacuated bed of particles by using concepts from the kinetic theory of gases [44]. They considered the flux of precursor molecules through the top surface of a bed of particles and calculated the time required to saturate the bed. Their analysis showed that the time required to saturate the surface was given by Equation (1):

$$\frac{t}{kT} = \frac{3}{4}\frac{\pi S}{r_c^2\,\Delta P}\sqrt{\frac{M}{2\pi RT}}\,l_c^2 \tag{1}$$

In this equation, r_c is the radius of the particles or pores, S is the number of sites per surface area, l_c is the length (or depth) of the bed, M is the molecular weight of the precursor, and ΔP is the dosing pressure of the precursor. This analysis takes into account that, during precursor exposure, the gas must adsorb from the top of the bed, saturate those particles first, and can only then progress deeper into the pores. In their analysis, Longrie et al. pointed out that the adsorption time could be hundreds of hours if the experimental parameters are not chosen properly. Fortunately, the equation provides criteria for minimizing the required exposure times. It is especially important that the diffusion length be kept short. This can be accomplished by forming the powders into thin wafers, as shown in Figure 3, rather than having a freestanding bed of powder. Alternatively, as the same research group has shown in a different publication, ALD can be performed on thin catalyst films [22]. Increasing the pressure of the precursor also can significantly decrease the required exposure time. In some cases, the development of new, highly volatile precursors may be necessary [57].

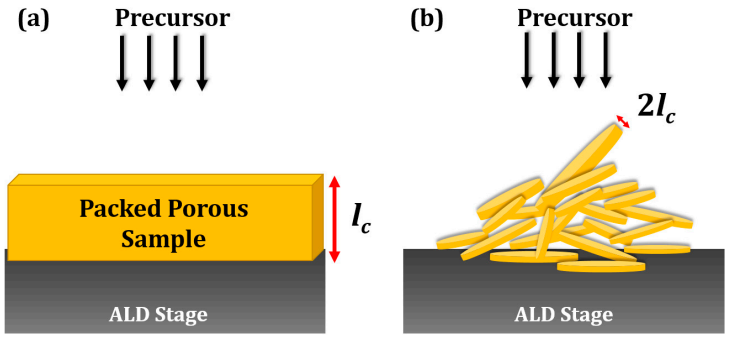

Figure 3. Illustration of a static ALD system to compare (**a**) a porous sample in a packed bed with depth, l_c; and (**b**) a porous sample of the same mass pressed into pellets with depth, l_c.

In addition to affecting the exposure time, high-surface-area samples also require considerably larger amounts of the precursor. Required precursor amounts for a single ALD exposure can be

estimated by assuming a 100 m^2/g powder with an adsorption site density of ~10^{18} sites/m^2 [58]. To coat one gram of such powder, the amount of precursor required for a uniform monolayer coverage is ~10^{-4} moles. This is a non-trivial amount to introduce by gas-phase exposure at low pressures.

2.2. Purging the Excess Precursor and Reaction Byproducts from the Sample

After the exposure step, excess precursor molecules and byproducts from the substrate must be removed by purging. This can be the longest step in the ALD cycle [41,42]. In order to increase the production rate of wafers in the semiconductor industry, flow ALD systems with He as the carrier gas are used to flush gas-phase and physisorbed molecules from the sample [21,41]. This is not trivial for a porous sample, since the excess precursor molecules and byproducts in the pores must diffuse to the exterior of the pore while in the presence of the carrier gas molecules. Diffusion of the excess precursor out of a porous sample will be described by a similar set of equations as outlined above for precursor exposure, but with several additional complications.

First, for very small pores, the saturation pressure of the precursor could be lowered due to capillarity, which leads to condensation locally in the sample. This reduces the driving force for diffusion of the precursor out of the bed. That driving force in Equation (1) is ΔP, the difference between the partial pressure in the pores and the partial pressure in the carrier-gas purge. A second additional complication is that desorption rates in porous materials are much slower than those from flat samples when the desorbing species can readsorb on other parts of the sample. Even when purging using an infinitely high carrier-gas flow rate, the effective desorption rate from the pores will be given by Equation (2) [59]:

$$k_{\text{eff}} = \frac{\pi^2 D}{S k_a l_c^2} k_{\text{d}} \tag{2}$$

In this equation, D is the diffusivity of the precursor, S is again the surface area of the substrate, and k_a is the adsorption rate constant. In the derivation of this equation, which was developed to describe desorption from porous materials into a vacuum, it was shown that the ratio of the effective desorption rate constant, k_{eff}, to the intrinsic desorption rate constant, k_{d}, can easily be much less than 10^{-6} for common catalyst powders. This implies that purging a porous sample of excess precursor molecules can be slow.

Obviously, when the purging step is incomplete, physisorbed precursor molecules may remain within the pore. Introducing the next reactant will lead to the reaction of these condensed species. Among the possible consequences of having condensed films in the pores are: (1) the formation of non-uniform films; (2) the formation of porous films; and (3) the production of films that are much thicker than would be expected for ALD. The reaction of condensed films has been invoked as an explanation for the thick porous films formed by ALD procedures in SOFC electrodes [48].

2.3. Gaseous Reactants to Remove Ligands and to Regenerate Sites

After purging, the active sites on the surface of the substrate must be regenerated through the removal of the ligands on the chemisorbed precursor molecules. There are standard methods for removing the ligands that work quite well for flat samples, usually through substitution of the ligands or complete combustion [53]. For example, we have already discussed the reaction of the adsorbed precursor for TMA with H_2O to remove the remaining methyl groups. For combustion of the ligands, it is common to use oxidizers such as H_2O_2 or O_3 [16].

However, ligand removal on porous samples is considerably more difficult, in part because there are more precursor ligands to remove. For many ligands, O_2 is not an effective oxidizer at ALD temperatures. For O_3 and H_2O_2, transport and concentration issues will often be a problem. While the principles behind the transport of O_3 and H_2O_2 are similar to those discussed earlier for the precursor adsorption step [22]; there is the added complication that these reactive species have limited lifetimes, and are typically present in small concentrations. For example, the half-life of ozone in air at 250 °C is only 1.5 s, and is much lower in the presence of catalytic materials [60]. If the time required for the

reactant to diffuse into the sample is long, this is obviously a problem. The maximum concentration of ozone reported in a typical industrial ozone generator is also only ~20% under pure O_2 flow. This leads to issues of dilution and additional diffusion limitations. Furthermore, for $La(TMHD)_3$, the precursor that was discussed earlier for preparing La_2O_3 films, the amount of oxidant required for the complete combustion of the ligands is very large, which can in turn lead to additional diffusion limitations. Incomplete removal of the ligands will almost certainly influence the growth behavior for subsequent ALD cycles [61].

Two interesting alternatives for ALD in porous materials are NO_2 [37] and oxygen plasmas [62,63]. NO_2 is a strong oxidant that can be produced in high concentrations, and has been used as a means to perform a low-temperature oxidation of soot that would normally require oxidation at 600 °C [64]. NO_2 has been successfully demonstrated to remove ligands from the chemisorbed precursor $La(THMD)_3$ on Al_2O_3 at less than 300 °C [37]. O_2 plasmas are also good oxidizers, and can be generated *in situ* using a radio-frequency generator. The partial removal of coke from zeolite catalysts at low temperatures was demonstrated in the 1980s using an oxygen plasma [65]. Recent advances in the technique have seen oxygen plasmas generated at atmospheric pressures, with the complete removal of coke from Pt–Sn/Al_2O_3 catalysts and H-ZSM-5 catalysts at near room temperature [62,63].

2.4. Purging the Excess Reactants and Reaction Byproducts

Finally, the ALD cycle is completed with the purging of the byproducts and the excess ligand removal reactants. Since each ALD cycle is irreversible and involves reactions at saturation, the amount of material deposited per area should be the same on flat or complex substrates, provided that sufficient precursors chemisorb on the entirety of the surface, complete purging is achieved, and the ligands are successfully removed regardless of reactor design.

3. ALD Reactor Designs for Catalysts and SOFC Electrodes

The principles behind ALD are the same in all of the systems. However, the use of a carrier gas as depicted in Figure 1 is not ideal for catalysts and high-surface-area samples. Two alternative reactor designs have been used for this situation.

The first is the *static reactor*, which is shown schematically in Figure 4a. The term "static" is used here to refer to the sample inside the reactor being exposed to non-flowing (i.e., static) precursors. The reactor itself can be rotating, or the particles inside the reactor can be agitated in various other ways [44,66,67], although simple static reactors without any moving parts have successfully been used to coat catalysts and SOFC electrodes [68–75]. In a static reactor, the sample is held in a sealed vessel that can be evacuated. Exposure to the precursor is performed in the same way that any adsorption would be performed, and the purge cycles would be performed by simply evacuating the sample. A purge gas may still be used in between precursor exposure steps [76], although it is not required. Compared to flow reactors—such as the one shown in Figure 1, where a significant portion of the precursor passes the substrate unreacted, making the coating of samples requiring large reactant exposures impractical—precursor utilization in static reactors can reach very high levels [43,44]. As mentioned earlier, the practicality of using a static system for large samples has been questioned due to the possible requirement for long exposures to saturate the surface with the precursor. However, since only a few ALD cycles are required to reach substantial weight loadings (see Section 1.4), long exposure and purge times (on the order of 10's of minutes or perhaps even hours) may be acceptable, as demonstrated by the fixed bed static reactor design developed by researchers at BASF [56]. It should be noted that exposure times can be shortened by using agitated or rotating bed reactors [44,66,67], using thin pelletized samples (Figure 3) [70–73], and increasing precursor partial pressures [56,57].

The second reactor design that has been used for coating porous materials by ALD is the *fluidized bed reactor*, which is shown schematically in Figure 4b. In this reactor type, a bed of particles is suspended in the flow of a carrier gas, causing the particles to behave like a liquid [77]. Fluidization

ensures high rates of physical mixing, as well as rapid heat transfer between the phases. While the fluidization of micron-sized particles is a mature technology that is employed on an industrial scale, the fluidization of nanopowders is a relatively new field. Nanoparticles fluidize as highly porous soft agglomerates that are several hundreds of microns in diameter (Figure 5), and continuously break apart and re-assemble due to attrition in the bed [44,49,77–79].

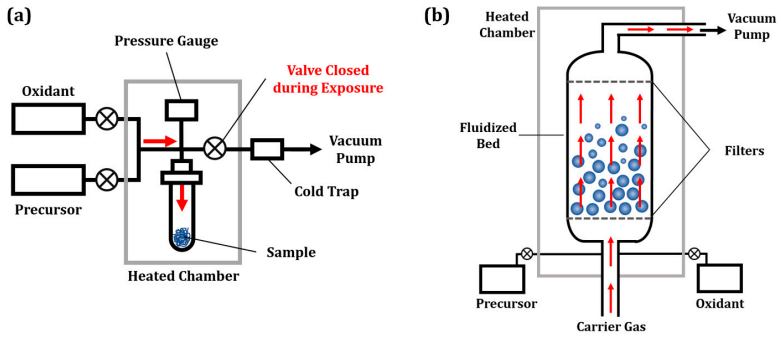

Figure 4. (**a**) Simplified schematic of a static ALD reactor designed for coating porous samples. The red arrows indicate the diffusion of gaseous reagents into the sample chamber during the exposure step. The valve to the vacuum is kept closed during the exposure step. (**b**) Simplified schematic of a fluidized bed ALD reactor designed for deposition on porous samples. The red arrows indicate the movement of the carrier gas through the sample to the exhaust.

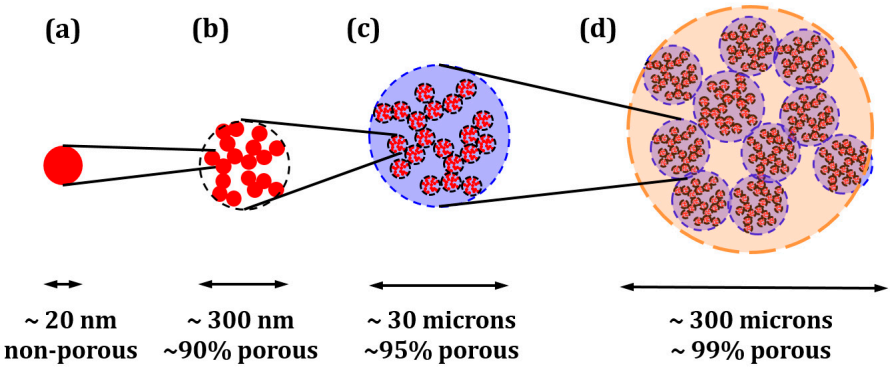

Figure 5. The structure of nanoparticle agglomerates during fluidization: (**a**) primary particles; (**b**) aggregates; (**c**) simple agglomerates; and (**d**) complex agglomerates. Size and porosity estimates are based on the structure of a common catalyst material, Degussa P-25 TiO_2. Based on data from [49,76,77].

Therefore, in order to reach the surface and react, a precursor molecule in the bubble phase typically needs to traverse over distances that are several orders of magnitude longer than the diameter of the primary particles via diffusion. The effectiveness of precursor use is highly dependent on operating pressure (the lower, the better), reactor height (the longer, the better), average bubble size (the smaller, the better), agglomerate structure (the smaller and mechanically weaker, the better), as well as the chosen ALD chemistry (the smaller the precursor molecules, the better) [44,49]. In a thorough modeling study, Grillo et al. demonstrated that reaching very high precursor utilizations is possible in properly designed fluidized bed ALD reactors used in proper operating conditions [49]. However, an important implication of this is that a reactor that is designed for coating one catalyst material with an ALD coating based on a specific ALD precursor/reactant pair is almost certainly not the optimal design for coating the same material using a different ALD chemistry, let alone for coating a different catalyst material with different fluidization characteristics and specific surface area. Thus far, studies on precursor utilization have largely focused on the TMA/H_2O process [49,77], which, as mentioned earlier, is very close to being an ideal ALD process. However, the molecular weight of most

other ALD precursors is significantly higher, and their sticking coefficients (i.e., the probability that the precursor molecule hitting the surface will react or "stick") can be orders of magnitude lower than for TMA [43]. In other words, while some encouraging examples exist, achieving commercially viable precursor utilizations in fluidized bed ALD reactors is certainly not trivial.

4. Atomic Layer Deposition (ALD) in Catalyst Design and Synthesis

As pointed out in earlier sections, ALD has found application in a number of areas of catalyst synthesis. Since this literature has already been reviewed by a number of groups [25–27], we will focus here on three areas in which we believe ALD can have a particularly important role.

4.1. Formation of Isolated Sites

As exhaustively demonstrated by a plethora of studies, metal-based heterogeneous catalysis is strongly dependent on the size of the metal particles. Tuning the size of the metal catalysts with nanometric precision enables a correlation between size and activity at a fundamental level. Furthermore, the current tendency in metal catalyst synthesis is to reduce the size of the metal particles, thus maintaining the exposed surface area while reducing the metal loading. ALD techniques, under appropriate conditions, allow the reduction of the size of the metal catalyst to a subnanometric level. Ultra-small Pd nanoparticles prepared via ALD can be precisely tailored to be in the range of 0.8 nm to 2.2 nm. The trend of increasing activity with metal size has been nicely confirmed for methanol decomposition [80]. ALD synthesis also underpins a strategy for the improved dispersion of the metal particles on the support compared with standard techniques such as impregnation. This factor is instrumental for a higher overall performance [81].

The extrapolation towards smaller and smaller particles leads to the ideal case where the metal atoms are isolated, allowing examination of the catalytic characteristics and concomitantly providing a unique catalytic behavior. The previous examples do not rule out the possibility of forming, together with the small metal particles, isolated metal atoms or small clusters. The preparation of a catalyst consisting of single metal atoms has been demonstrated in a number of emergent reports [82]. For many ALD precursors, the ligands are relatively large, and the resulting coverage of the metal atoms can be very low. The correct choice of the metal ligand could be a parameter to increase the single metal sites during the ALD process. Values below 10^{18} atom/m^2 per cycle are not uncommon [58]. An implication of this is that a single ALD cycle may be able to form isolated atoms or a small metal cluster. Increasing the number of cycles would cause an enhancement of the metal loading and the size of the metal clusters [45,83].

Apart from ligand choice, several other approaches can be pursued to afford isolated atoms. For instance, tuning the modification of graphene layers with oxygen functionalities was key to the deposition of single Pd atoms via ALD, as shown on Figure 6. The isolated Pd atoms displayed among the highest selectivities ever reported for the hydrogenation of 1,3-butadiene, as explained by the authors in terms of a different 1,3-butadiene adsorption mode on the Pd atoms, which was triggered by the steric effect of the diene on the single atom [46]. Demonstrating the presence of isolated atoms is not trivial; it requires advanced characterization techniques, including microscopic techniques above all.

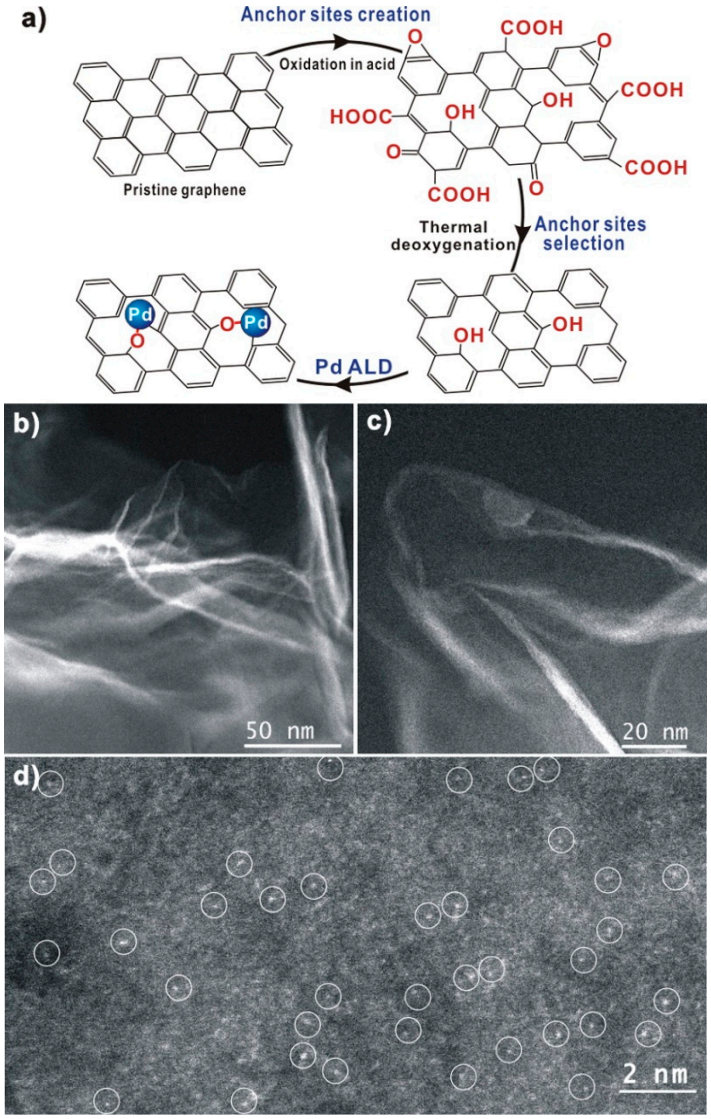

Figure 6. Synthetic scheme (**a**) and high-angle annular dark-field scanning transmission electron microscopy (HAADF-STEM) images of Pd1/graphene at low (**b**,**c**) and high (**d**) magnifications. Atomically dispersed Pd atoms in the image (**d**) are highlighted by the white circles [46]. Reprinted with permission from *J. Am. Chem. Soc.* **2015**, *137*, 10484–10487. Copyright (2015) American Chemical Society.

4.2. High-Surface-Area Functional Oxides

Many functional oxides, including the important example of ceria–zirconia mixed oxides, typically have surface areas of only 2 m^2/g under operating conditions [84]. It is obviously desirable to maximize surface area in order to improve catalytic performance, while providing a better stability of the functional oxide. These two conditions are commonly fulfilled dispersing the functional oxide on large surface area inert support, typically through impregnation methods. However, in many cases, the dispersed oxide undergoes aggregation of the crystallites and a partial collapse of the surface area. ALD is becoming a particularly popular strategy to circumvent this problem. In practice, the strategy consists of depositing a thin film of the oxide of interest onto an inert but stable support with a large surface area using ALD. The resulting material shows a much larger surface area of the functional oxide, which also turns out to be thermally stable, as shown in the preparation of Al_2O_3–CeO_2 supports, which had improved catalytic activity towards water–gas shift with respect to bulk ceria [72]. The achievement of one monolayer of functional oxide is critical to this strategy,

as it is then the platform to establish the correct conditions of each individual ALD cycle in order to have a precise number of layers. Practical applications dictate that the film thickness be no greater than approximately 1 nm in order to maintain high surface areas, good stability, and activity. The ALD strategy is rather flexible, and a range of oxides and mixed oxides can be prepared, provided that suitable conditions are found. Fe_2O_3 films with high surface areas have been deposited on Al_2O_3; however, the synthesis required the employment of a static system [51,71]. Microscopic evidence, together with energy-dispersive X-ray spectroscopy (EDS) element mapping confirmed the difference in uniformity of the ALD sample versus the impregnated sample, with the latter presenting large aggregates of the Fe_2O_3 (Figure 7).

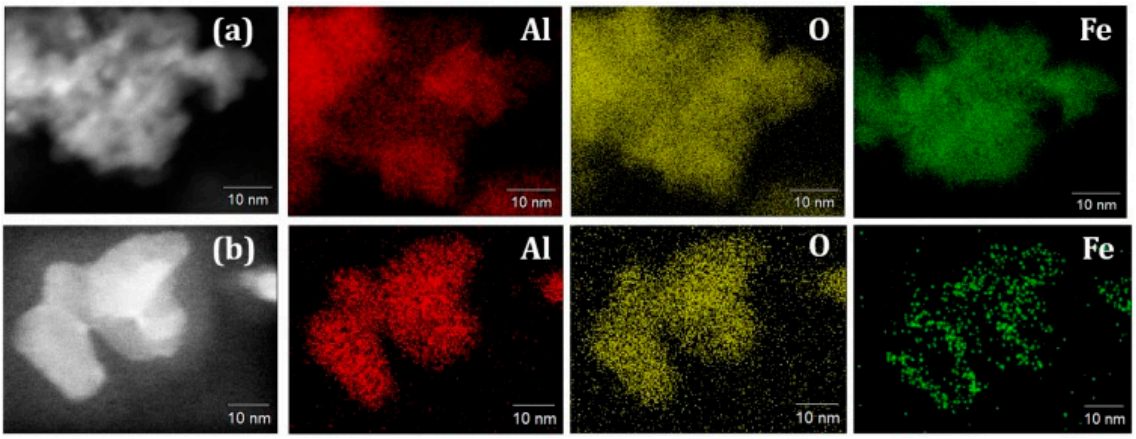

Figure 7. Representative HAADF-STEM images with corresponding EDS mapping of (**a**) Fe_2O_3 added onto a high-surface area Al_2O_3 support by metal salt impregnation and (**b**) Fe_2O_3 deposited onto the Al_2O_3 support by ALD [71]. EDS mapping of Al, O, and Fe shows rich Fe signals on the edges on the ALD-modified Al_2O_3 support, while there was no preferential distribution of Fe on the infiltrated sample. Reprinted with permission from *Appl. Catal. A* **2017**, *534*, 70–77. Copyright (2017) Elsevier.

The ALD approach is also applicable to mixed oxides, such as for example CeO_2–ZrO_2 mixed oxides, by alternating suitable Ce and Zr precursors during ALD cycles [73,85]. Although high surface area perovskites can be prepared by combustion synthesis [86,87], $LaFeO_3$ films with the perovskite structure were also prepared by ALD [38].

4.3. Coated Surfaces for Enhanced Stability

Another important potential application of ALD is in stabilizing metal particles by forming an "overcoat" of a porous layer to prevent sintering. Strategies other than ALD have also been recently reported, such as a layer-by-layer solution-based approach [88], but ALD offers better control and has more versatility [53]. A few studies have reported that the coating of metal nanoparticles through ALD is also compatible with harsh conditions such as high temperatures, thus implying stability for catalytic processes requiring high temperatures [89,90]. It is obvious that the coverage of the metal nanoparticles with thin layers of oxides must prevent sintering while not compromising the accessibility of the active site. For this reason, surface area and porosity of the deposited oxide must be controlled. Typically, only a few ALD cycles are performed in order to have ultrathin overcoats that minimize mass transfer resistance (Figure 8). Large pores may imply only a partial coverage of the metal particles. This fact is particularly important when the material is subjected to calcination treatments [70], which are therefore a useful tool to further modify the overcoat textural properties, allowing a fine-tuning of the catalytic features. Indeed, it has been reported that calcination is fruitful for producing an increase of activity of the catalyst in some cases, with the metal being accessible, while still protected [91].

In addition to protection against sintering, the ALD overcoat can also suppress coking in those catalytic reactions involving a carbon-containing reactant. In some cases, the coking must be avoided

by using thicker layers of protective metal oxide in order to dramatically improve the stability of the system. However, once again, the ALD deposited coverage must possess suitable porosity in order not to compromise activity (which in some cases may still be lower). Metal oxides that are able to provide adequate porosity must be chosen, such as the case of Pd nanoparticles coated by Al_2O_3, where the overcoat was shown to possess microporosity, making the catalyst active (and significantly more stable) in the oxidative dehydrogenation of ethane to ethylene [92].

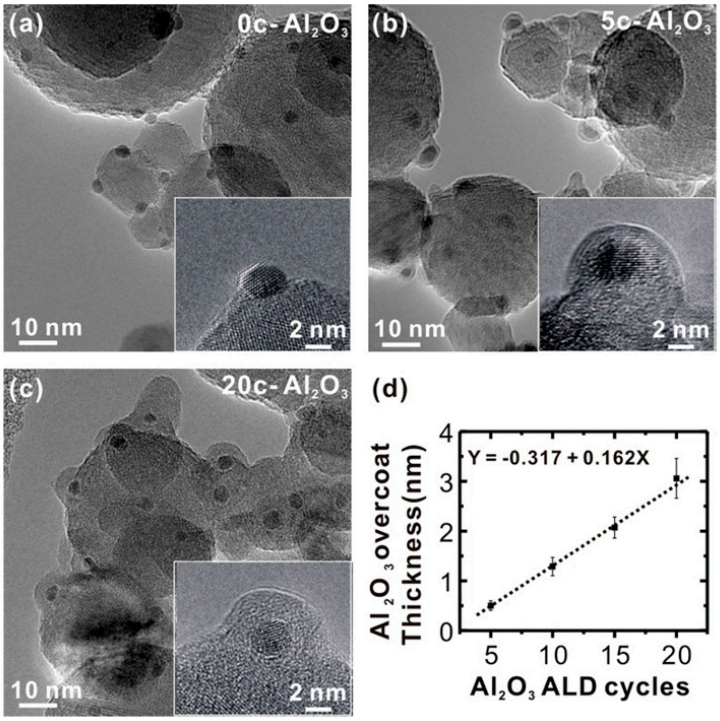

Figure 8. TEM images of Pd/Al_2O_3 catalysts on spherical alumina support following different numbers of ALD Al_2O_3 overcoating cycles (insets show higher magnification images). (**a**) Without overcoating; (**b**) five cycles Al_2O_3; (**c**) 20 cycles Al_2O_3; (**d**) thickness of Al_2O_3 overcoats versus ALD cycles [89]. Reprinted with permission from *Chem. Mater.* **2012**, *24*, 2047–2055. Copyright (2012) American Chemical Society.

5. Applications to SOFC Electrodes

ALD has the potential to impact SOFC fabrication in a number of ways, and efforts have gone into applying it to problems in both electrolytes and electrodes. Since electrolytes tend to be relatively thick for ALD, most of the work on electrolytes involves modifying the surfaces of the electrolyte [93] or adding a barrier layer to electrolytes to prevent reactions with the cathode materials [20,94–97]. ALD has also been used to deposit Pt current collectors onto an existing SOFC cathode [98]. Each of these applications involves the preparation of films on flat surfaces, and can use conventional ALD methods. We will therefore not discuss these applications here, and instead simply refer the reader to other reviews [20,22,23].

5.1. Modification of SOFC Cathodes

Since initial and long-time SOFC performance are usually limited by the cathode, the electrode where the O_2 reduction reaction (ORR) takes place, the most important potential role for ALD in SOFC fabrication involves the modification of this component. SOFC cathodes are almost always based on electronically conductive perovskites, such as $La_{0.6}Sr_{0.4}Co_{0.2}Fe_{0.8}O_{3-\delta}$ (LSCF), $La_{0.6}Sr_{0.4}CoO_{3-\delta}$ (LSCo), $La_{0.6}Sr_{0.4}FeO_{3-\delta}$ (LSF), or $La_{0.6}Sr_{0.4}MnO_{3-\delta}$ (LSM) (note: Sr is added in order to introduce

oxygen vacancies, but the doping level can be varied). In addition to having electronic conductivity, these materials also have oxygen ion conductivity, which allows oxygen ions that are transported through the electrolyte to be formed at some distance from the electrolyte, and enables them to adsorb gas-phase O_2 dissociatively at lattice vacancies. While thin film cathode materials, such as LSM [99] and LSF [100] have been deposited using ALD, the structure of state-of-the-art porous cathodes are more complex, consisting of composites of the perovskite and the material used in the electrolyte [101,102].

One area in which ALD can have an impact on SOFC cathodes is in modifying and stabilizing the electrode structure. For example, Huang et al. examined nanostructured LSCo electrodes that had been coated with a porous layer, ~10 nm thick, of ZrO_2 by ALD (Figure 9a) [103]. They showed that a high ORR activity could be successfully retained on these electrodes for 4000 h at 700 °C. The degradation rate of the ALD-ZrO_2 modified LSCo cathode was only $1/18^{th}$ of the uncoated baseline, as shown in Figure 9b. The authors of that study attributed the retained ORR activity to the multifunctionality of the ALD-ZrO_2 layer, i.e., nanoporosity, mixed oxide ion and electronic conductivity, physical confinement to coarsening, and suppression of Sr segregation. These results were confirmed in another study that also observed enhanced cathode performance upon the deposition of relatively thick, porous ZrO_2 films [30].

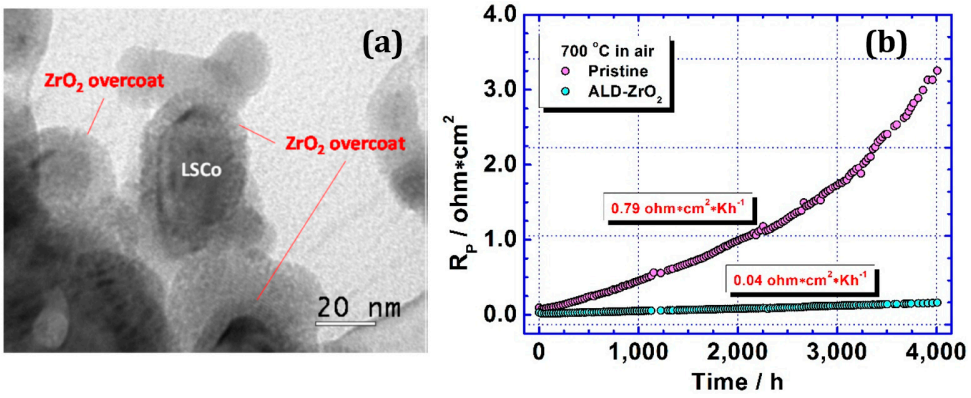

Figure 9. (**a**) ALD-ZrO_2 overcoat on $La_{0.6}Sr_{0.4}CoO_{3-\delta}$ (LSCo) nanoparticles. (**b**) Comparison of area specific polarization resistance between uncoated and coated samples [103]. Reprinted with permission from *Nano Lett.* **2013**, *13*, 4340–4345. Copyright (2013) American Chemical Society.

A third study on ZrO_2 coatings on SOFC cathodes, where the film was deposited in a static system [37], helps to demonstrate the importance of deposition conditions when modifying porous electrodes. In that study, SOFC cathodes were modified by a dense, 1-nm ALD film of ZrO_2. Even with this very thin film, the cathodes showed a strong decrease in performance, which was apparently due to the simple blocking of oxygen adsorption sites on the LSF part of the cathode. The major difference between this and the earlier studies that showed enhanced performance with 10-nm ZrO_2 films was that the earlier studies used a carrier gas to introduce the precursor to the electrode and purge excess from the electrode, while the later study exposed the sample to a pure precursor vapor and purged the sample by evacuation. Film growth rates in the studies performed using a carrier gas were reported to be ~0.6 nm/cycle, while the growth rate in a static system was 0.02 nm/cycle. The very high growth rates in the earlier studies imply that the fundamental processes that were responsible for ALD were very different.

Interestingly, the later study showed a decrease in cathode performance following the deposition of either ZrO_2 or Fe_2O_3 films onto lanthanum strontium ferrite–yttria-stabilized zirconia (LSF–YSZ) composite cathodes, but also showed that improved performance could be achieved by the ALD of La_2O_3 and La_2O_3–Fe_2O_3 ($LaFeO_3$) mixtures. When films of La_2O_3 were greater than one monolayer (~1 nm), the cathode impedance again increased (i.e., made the performance worse); however, submonolayers of LaO_x significantly decreased the impedance. This result suggests that the original

LSF phase may have been A-site deficient at the surface; so, small amounts of La could improve performance by completing the perovskite structure. Results following the deposition of La_2O_3–Fe_2O_3 mixtures also showed enhanced cathode performance, even for relatively thick films. The important conclusion from this study is that ALD may be used to enhance O_2 adsorption sites. Other groups are also investigating the ALD modification of SOFC cathodes by catalytically active oxides [104]. Finally, there is a growing interest in using perovskite powders with their surface modified by ALD, as drop-in substitutes for unmodified powders in commercial SOFC systems [105].

Chang et al. also observed a beneficial effect of ALD-ZrO_2 coatings on a functional SOFC cathode for ultrathin YSZ layers deposited on a porous Pt cathode by ALD [95]. In this case, the thin YSZ coating prevented Pt sintering, maintaining a porous morphology of the underlying Pt during 500 °C operation. More interestingly, the YSZ coating also improved the ORR (oxygen reduction reaction) activity by a factor of 2.5. The authors argued that the improvement was due to an enlarged three-phase boundary, especially near the Pt-electrolyte interface, due to the addition of an ion-conducting component to the Pt electrode. In related works, Karimaghaloo et al. and Liu et al. also showed that YSZ coatings on porous Pt cathodes helped retain the ORR activity by suppressing the agglomeration of the porous Pt [106,107].

5.2. Modification of SOFC Anodes

The most common material used for SOFC anodes is a mixture of Ni and YSZ, which is known as Ni–YSZ cermet (ceramic–metallic composite) [108]. Ni provides the conductivity and catalytic activity, while YSZ provides oxygen ion conductivity and helps maintain porosity. These electrodes perform very well, but there are problems with the oxidation of Ni when the flow of reducing gas to the anode is interrupted, and carbon formation at low steam-to-carbon ratios [109,110]. Both oxidation and carbon formation can result in a catastrophic loss of cell performance. ALD is ideal for coating the Ni phase with a thin overcoat to suppress the agglomeration and oxidation of the underlying Ni [111]. A similar approach would seem to be ideal for depositing ceria to prevent carbon formation [112].

6. Summary and Outlook

ALD is an exciting tool that allows the structure and composition of surfaces to be controlled on the atomic scale in the preparation of heterogeneous catalysts and SOFC electrodes. Conventional ALD approaches have been successful in growing conformal films on flat surfaces for the semiconductor industry, but the approaches that are commonly used in those applications, where reactants are rapidly cycled to the substrate, may lead to serious issues associated with the diffusion limitations of materials into the porous samples. The elimination of diffusion gradients, efficient use of precursors, and ligand removal with less reactive precursors are the major factors that need to be controlled for the successful deposition of films on porous samples. With the appropriate choice of experimental parameters, ALD offers exciting possibilities to modify heterogenous catalysts and SOFC electrodes.

Acknowledgments: Tzia Ming Onn and Raymond J. Gorte are grateful to the Department of Energy, Office of Basic Energy Sciences, Chemical Sciences, Geosciences and Biosciences Division, Grant No. DE-FG02-13ER16380 for support of this work.

Author Contributions: Tzia Ming Onn, Rainer Küngas, Paolo Fornasiero, Kevin Huang, and Raymond J. Gorte contributed to the write-up of the different sections of the review. Raymond J. Gorte supervised the write-up of the paper.

Conflicts of Interest: The authors declare no conflict of interest.

References

1. Ma, Z.; Zaera, F. Heterogeneous catalysis by metals. In *Encyclopedia of Inorganic and Bioinorganic Chemistry*; Wiley: New York, NY, USA, 2014; pp. 1–16.
2. Di Monte, R.; Kašpar, J. On the role of oxygen storage in three-way catalysis. *Top. Catal.* **2004**, *28*, 47–57. [CrossRef]

3. Morikawa, A.; Suzuki, T.; Kanazawa, T.; Kikuta, K.; Suda, A.; Shinjo, H. A new concept in high performance ceria–zirconia oxygen storage capacity material with Al_2O_3 as a diffusion barrier. *Appl. Catal. B Environ.* **2008**, *78*, 210–221.
4. Gorte, R.J. Ceria in catalysis: From automotive applications to the water–gas shift reaction. *AIChE J.* **2010**, *56*, 1126–1135.
5. Montini, T.; Melchionna, M.; Monai, M.; Fornasiero, P. Fundamentals and catalytic applications of CeO_2-based materials. *Chem. Rev.* **2016**, *116*, 5987–6041. [CrossRef] [PubMed]
6. Shekhar, M.; Wang, J.; Lee, W.-S.; Williams, W.D.; Kim, S.M.; Stach, E.A.; Miller, J.T.; Delgass, W.N.; Ribeiro, F.H. Size and support effects for the water–gas shift catalysis over gold nanoparticles supported on model Al_2O_3 and TiO_2. *J. Am. Chem. Soc.* **2012**, *134*, 4700–4708. [CrossRef] [PubMed]
7. Cargnello, M.; Doan-Nguyen, V.V.; Gordon, T.R.; Diaz, R.E.; Stach, E.A.; Gorte, R.J.; Fornasiero, P.; Murray, C.B. Control of metal nanocrystal size reveals metal-support interface role for ceria catalysts. *Science* **2013**, *341*, 771–773. [PubMed]
8. Zhu, Y.; Ramasse, Q.M.; Brorson, M.; Moses, P.G.; Hansen, L.P.; Kisielowski, C.F.; Helveg, S. Visualizing the stoichiometry of industrial-style Co–Mo–S catalysts with single-atom sensitivity. *Angew. Chem. Int. Ed.* **2014**, *53*, 10723–10727. [CrossRef] [PubMed]
9. Kanno, D.; Shikazono, N.; Takagi, N.; Matsuzaki, K.; Kasagi, N. Evaluation of SOFC anode polarization simulation using three-dimensional microstructures reconstructed by FIB tomography. *Electrochim. Acta* **2011**, *56*, 4015–4021. [CrossRef]
10. Bidrawn, F.; Kim, G.; Aramrueang, N.; Vohs, J.; Gorte, R. Dopants to enhance SOFC cathodes based on Sr-doped $LaFeO_3$ and $LaMnO_3$. *J. Power Sources* **2010**, *195*, 720–728. [CrossRef]
11. Kiebach, R.; Knöfel, C.; Bozza, F.; Klemensø, T.; Chatzichristodoulou, C. Infiltration of ionic-, electronic- and mixed-conducting nano particles into $La_{0.75}Sr_{0.25}MnO_3$-$Y_{0.16}Zr_{0.84}O_2$ cathodes—A comparative study of performance enhancement and stability at different temperatures. *J. Power Sources* **2013**, *228*, 170–177. [CrossRef]
12. Adijanto, L.; Sampath, A.; Yu, A.S.; Cargnello, M.; Fornasiero, P.; Gorte, R.J.; Vohs, J.M. Synthesis and stability of Pd@CeO_2 core–shell catalyst films in solid oxide fuel cell anodes. *ACS Catal.* **2013**, *3*, 1801–1809. [CrossRef]
13. Ding, D.; Li, X.; Lai, S.Y.; Gerdes, K.; Liu, M. Enhancing SOFC cathode performance by surface modification through infiltration. *Energy Environ. Sci.* **2014**, *7*, 552–575. [CrossRef]
14. Yang, L.; Wang, S.; Blinn, K.; Liu, M.; Liu, Z.; Cheng, Z.; Liu, M. Enhanced sulfur and coking tolerance of a mixed ion conductor for SOFCs: $BaZr_{0.1}Ce_{0.7}Y_{0.2-x}Yb_xO_{3-\delta}$. *Science* **2009**, *326*, 126–129. [CrossRef] [PubMed]
15. Yang, L.; Choi, Y.; Qin, W.; Chen, H.; Blinn, K.; Liu, M.; Liu, P.; Bai, J.; Tyson, T.A.; Liu, M. Promotion of-mediated carbon removal by nanostructured/interfaces in solid oxide fuel cells. *Nat. Commun.* **2011**, *2*, 357. [CrossRef] [PubMed]
16. Puurunen, R.L. Surface chemistry of atomic layer deposition: A case study for the trimethylaluminum/water process. *J. Appl. Phys.* **2005**, *97*, 121301. [CrossRef]
17. Haukka, S.; Lakomaa, E.-L.; Suntola, T. Adsorption controlled preparation of heterogeneous catalysts. *Stud. Surf. Sci. Catal.* **1998**, *120*, 715–750.
18. Ivers-Tiffée, E.; Weber, A.; Herbstritt, D. Materials and technologies for SOFC-components. *J. Ceram. Soc.* **2001**, *21*, 1805–1811. [CrossRef]
19. Jacobson, A.J. Materials for solid oxide fuel cells. *Chem. Mater.* **2009**, *22*, 660–674. [CrossRef]
20. Cassir, M.; Ringuedé, A.; Niinistö, L. Input of atomic layer deposition for solid oxide fuel cell applications. *J. Mater. Chem.* **2010**, *20*, 8987–8993. [CrossRef]
21. George, S.M. Atomic layer deposition: An overview. *Chem. Rev.* **2010**, *110*, 111–131. [CrossRef] [PubMed]
22. Detavernier, C.; Dendooven, J.; Sree, S.P.; Ludwig, K.F.; Martens, J.A. Tailoring nanoporous materials by atomic layer deposition. *Chem. Soc. Rev.* **2011**, *40*, 5242–5253. [CrossRef] [PubMed]
23. Marichy, C.; Bechelany, M.; Pinna, N. Atomic layer deposition of nanostructured materials for energy and environmental applications. *Adv. Mater.* **2012**, *24*, 1017–1032. [CrossRef] [PubMed]
24. Van Delft, J.; Garcia-Alonso, D.; Kessels, W. Atomic layer deposition for photovoltaics: Applications and prospects for solar cell manufacturing. *Semicond. Sci. Technol.* **2012**, *27*, 074002. [CrossRef]

25. Johnson, R.W.; Hultqvist, A.; Bent, S.F. A brief review of atomic layer deposition: From fundamentals to applications. *Mater. Today* **2014**, *17*, 236–246. [CrossRef]
26. Singh, J.A.; Yang, N.; Bent, S.F. Nanoengineering heterogeneous catalysts by atomic layer deposition. *Annu. Rev. Chem. Biomol. Eng.* **2017**, *8*, 41–62. [CrossRef] [PubMed]
27. O'Neill, B.J.; Jackson, D.H.; Lee, J.; Canlas, C.; Stair, P.C.; Marshall, C.L.; Elam, J.W.; Kuech, T.F.; Dumesic, J.A.; Huber, G.W. Catalyst design with atomic layer deposition. *ACS Catal.* **2015**, *5*, 1804–1825. [CrossRef]
28. Keuter, T.; Mauer, G.; Vondahlen, F.; Iskandar, R.; Menzler, N.H.; Vassen, R. Atomic-layer-controlled deposition of TEMAZ/O_2–ZrO_2 oxidation resistance inner surface coatings for solid oxide fuel cells. *Surf. Coat. Technol.* **2016**, *288*, 211–220. [CrossRef]
29. Gong, Y.; Patel, R.L.; Liang, X.; Palacio, D.; Song, X.; Goodenough, J.B.; Huang, K. Atomic layer deposition functionalized composite SOFC cathode $La_{0.6}Sr_{0.4}Fe_{0.8}Co_{0.2}O_{3-\delta}$-$Gd_{0.2}Ce_{0.8}O_{1.9}$: Enhanced long-term stability. *Chem. Mater.* **2013**, *25*, 4224–4231. [CrossRef]
30. Chen, Y.; Gerdes, K.; Song, X. Nanoionics and nanocatalysts: Conformal mesoporous surface scaffold for cathode of solid oxide fuel cells. *Sci. Rep.* **2016**, *6*, 32997. [CrossRef] [PubMed]
31. Wilson, C.; Goldstein, D.; McCormick, J.; Weimer, A.; George, S. Tungsten atomic layer deposition on cobalt nanoparticles. *J. Vac. Sci. Technol. A* **2008**, *26*, 430–437. [CrossRef]
32. Yang, N.; Yoo, J.S.; Schumann, J.; Bothra, P.; Singh, J.A.; Valle, E.; Abild-Pedersen, F.; Nørskov, J.K.; Bent, S.F. Rh–MnO interface sites formed by atomic layer deposition promote syngas conversion to higher oxygenates. *ACS Catal.* **2017**, *7*, 5746–5757. [CrossRef]
33. Pickrahn, K.L.; Park, S.W.; Gorlin, Y.; Lee, H.B.R.; Jaramillo, T.F.; Bent, S.F. Active MnO_x electrocatalysts prepared by atomic layer deposition for oxygen evolution and oxygen reduction reactions. *Adv. Energy Mater.* **2012**, *2*, 1269–1277. [CrossRef]
34. Martinson, A.B.; DeVries, M.J.; Libera, J.A.; Christensen, S.T.; Hupp, J.T.; Pellin, M.J.; Elam, J.W. Atomic layer deposition of Fe_2O_3 using ferrocene and ozone. *J. Phys. Chem. C* **2011**, *115*, 4333–4339. [CrossRef]
35. Hu, Q.; Wang, S.; Gao, Z.; Li, Y.; Zhang, Q.; Xiang, Q.; Qin, Y. The precise decoration of Pt nanoparticles with Fe oxide by atomic layer deposition for the selective hydrogenation of cinnamaldehyde. *Appl. Catal. B Environ.* **2017**, *218*, 591–599. [CrossRef]
36. Nieminen, M.; Putkonen, M.; Niinistö, L. Formation and stability of lanthanum oxide thin films deposited from β-diketonate precursor. *Appl. Surf. Sci.* **2001**, *174*, 155–166. [CrossRef]
37. Rahmanipour, M.; Cheng, Y.; Onn, T.M.; Donazzi, A.; Vohs, J.M.; Gorte, R.J. Modification of LSF-YSZ composite cathodes by atomic layer deposition. *J. Electrochem. Soc.* **2017**, *164*, F879–F884. [CrossRef]
38. Onn, T.M.; Monai, M.; Dai, S.; Fonda, E.; Montini, T.; Pan, X.; Graham, G.W.; Fornasiero, P.; Gorte, R.J. Smart Pd catalyst with improved thermal stability supported on high-surface-area $LaFeO_3$ prepared by atomic layer deposition. *J. Am. Chem. Soc.* **2018**. accepted. [CrossRef] [PubMed]
39. Haukka, S. ALD technology-present and future challenges. *ECS Trans.* **2007**, *3*, 15–26.
40. Raaijmakers, I.J. Current and future applications of ALD in micro-electronics. *ECS Trans.* **2011**, *41*, 3–17.
41. Elam, J.; Groner, M.; George, S. Viscous flow reactor with quartz crystal microbalance for thin film growth by atomic layer deposition. *Rev. Sci. Instrum.* **2002**, *73*, 2981–2987. [CrossRef]
42. Elers, K.E.; Blomberg, T.; Peussa, M.; Aitchison, B.; Haukka, S.; Marcus, S. Film uniformity in atomic layer deposition. *Chem. Vap. Depos.* **2006**, *12*, 13–24. [CrossRef]
43. Elam, J.; Routkevitch, D.; Mardilovich, P.; George, S. Conformal coating on ultrahigh-aspect-ratio nanopores of anodic alumina by atomic layer deposition. *Chem. Mater.* **2003**, *15*, 3507–3517. [CrossRef]
44. Longrie, D.; Deduytsche, D.; Detavernier, C. Reactor concepts for atomic layer deposition on agitated particles: A review. *J. Vac. Sci. Technol. A* **2014**, *32*, 010802. [CrossRef]
45. Sun, S.; Zhang, G.; Gauquelin, N.; Chen, N.; Zhou, J.; Yang, S.; Chen, W.; Meng, X.; Geng, D.; Banis, M.N. Single-atom catalysis using Pt/graphene achieved through atomic layer deposition. *Sci. Rep.* **2013**, *3*, 1775. [CrossRef]
46. Yan, H.; Cheng, H.; Yi, H.; Lin, Y.; Yao, T.; Wang, C.; Li, J.; Wei, S.; Lu, J. Single-atom Pd1/graphene catalyst achieved by atomic layer deposition: Remarkable performance in selective hydrogenation of 1, 3-butadiene. *J. Am. Chem. Soc.* **2015**, *137*, 10484–10487. [CrossRef] [PubMed]
47. Piernavieja-Hermida, M.; Lu, Z.; White, A.; Low, K.-B.; Wu, T.; Elam, J.W.; Wu, Z.; Lei, Y. Towards ALD thin film stabilized single-atom Pd1 catalysts. *Nanoscale* **2016**, *8*, 15348–15356. [CrossRef] [PubMed]

48. Lee, H.-Y.; An, C.J.; Piao, S.J.; Ahn, D.Y.; Kim, M.-T.; Min, Y.-S. Shrinking core model for knudsen diffusion-limited atomic layer deposition on a nanoporous monolith with an ultrahigh aspect ratio. *J. Phys. Chem. C* **2010**, *114*, 18601–18606. [CrossRef]
49. Grillo, F.; Kreutzer, M.T.; van Ommen, J.R. Modeling the precursor utilization in atomic layer deposition on nanostructured materials in fluidized bed reactors. *Chem. Eng. J.* **2015**, *268*, 384–398. [CrossRef]
50. Duan, C.-L.; Zhu, P.-H.; Deng, Z.; Li, Y.; Shan, B.; Fang, H.-S.; Feng, G.; Chen, R. Mechanistic modeling study of atomic layer deposition process optimization in a fluidized bed reactor. *J. Vac. Sci. Technol. A* **2017**, *35*, 01B102. [CrossRef]
51. Haukka, S.; Kytökivi, A.; Lakomaa, E.; Lehtovirta, U.; Lindblad, M.; Lujala, V.; Suntola, T. The utilization of saturated gas–solid reactions in the preparation of heterogeneous catalysts. *Stud. Surf. Sci. Catal.* **1995**, *91*, 957–966.
52. Wind, R.; George, S. Quartz crystal microbalance studies of Al_2O_3 atomic layer deposition using trimethylaluminum and water at 125 °C. *J. Phys. Chem. A* **2010**, *114*, 1281–1289. [CrossRef] [PubMed]
53. Miikkulainen, V.; Leskelä, M.; Ritala, M.; Puurunen, R.L. Crystallinity of inorganic films grown by atomic layer deposition: Overview and general trends. *J. Appl. Phys.* **2013**, *113*, 2. [CrossRef]
54. Ylilammi, M. Monolayer thickness in atomic layer deposition. *Thin Solid Films* **1996**, *279*, 124–130. [CrossRef]
55. Schindler, P.; Logar, M.; Provine, J.; Prinz, F.B. Enhanced step coverage of TiO_2 deposited on high aspect ratio surfaces by plasma-enhanced atomic layer deposition. *Langmuir* **2015**, *31*, 5057–5062. [CrossRef] [PubMed]
56. Strempel, V.; Naumann d'Alnoncourt, R.; Driess, M.; Rosowski, F. Atomic layer deposition on porous powders with in situ gravimetric monitoring in a modular fixed bed reactor setup. *Rev. Sci. Instrum.* **2017**, *88*, 074102. [CrossRef] [PubMed]
57. Kucheyev, S.; Biener, J.; Baumann, T.; Wang, Y.; Hamza, A.; Li, Z.; Lee, D.; Gordon, R. Mechanisms of atomic layer deposition on substrates with ultrahigh aspect ratios. *Langmuir* **2008**, *24*, 943–948. [CrossRef] [PubMed]
58. Lin, C.; Mao, X.; Onn, T.M.; Jang, J.; Gorte, R.J. Stabilization of ZrO_2 Powders via ALD of CeO_2 and ZrO_2. *Inorganics* **2017**, *5*, 65. [CrossRef]
59. Demmin, R.; Gorte, R. Design parameters for temperature-programmed desorption from a packed bed. *J. Catal.* **1984**, *90*, 32–39. [CrossRef]
60. Hutchings, G.; Copperthwaite, R.; Themistocleous, T.; Foulds, G.; Bielovitch, A.; Loots, B.; Nowitz, G.; Van Eck, P. A comparative study of reactivation of zeolite Y using oxygen and ozone/oxygen mixtures. *Appl. Catal.* **1987**, *34*, 153–161. [CrossRef]
61. Mackus, A.J.; MacIsaac, C.; Kim, W.-H.; Bent, S.F. Incomplete elimination of precursor ligands during atomic layer deposition of Zinc-Oxide, Tin-Oxide, and Zinc-Tin-Oxide. *J. Chem. Phys.* **2017**, *146*, 052802. [CrossRef] [PubMed]
62. HafezKhiabani, N.; Fathi, S.; Shokri, B.; Hosseini, S.I. A novel method for decoking of Pt–Sn/Al_2O_3 in the naphtha reforming process using RF and pin-to-plate DBD plasma systems. *Appl. Catal. A Gen.* **2015**, *493*, 8–16. [CrossRef]
63. Jia, L.; Farouha, A.; Pinard, L.; Hedan, S.; Comparot, J.-D.; Dufour, A.; Tayeb, K.B.; Vezin, H.; Batiot-Dupeyrat, C. New routes for complete regeneration of coked zeolite. *Appl. Catal. B Environ.* **2017**, *219*, 82–91. [CrossRef]
64. Stanmore, B.R.; Brilhac, J.-F.; Gilot, P. The oxidation of soot: A review of experiments, mechanisms and models. *Carbon* **2001**, *39*, 2247–2268. [CrossRef]
65. Bibby, D.; Milestone, N.; Patterson, J.; Aldridge, L. Coke formation in zeolite ZSM-5. *J. Catal.* **1986**, *97*, 493–502. [CrossRef]
66. McCormick, J.; Cloutier, B.; Weimer, A.; George, S. Rotary reactor for atomic layer deposition on large quantities of nanoparticles. *J. Vac. Sci. Technol. A* **2007**, *25*, 67–74. [CrossRef]
67. Cavanagh, A.S.; Wilson, C.A.; Weimer, A.W.; George, S.M. Atomic layer deposition on gram quantities of multi-walled carbon nanotubes. *Nanotechnology* **2009**, *20*, 255602. [CrossRef] [PubMed]
68. Lindblad, M.; Lindfors, L.P.; Suntola, T. Preparation of Ni/Al_2O_3 catalysts from vapor phase by atomic layer epitaxy. *Catal. Lett.* **1994**, *27*, 323–336. [CrossRef]
69. Anthony, S.Y.; Küngas, R.; Vohs, J.M.; Gorte, R.J. Modification of SOFC cathodes by atomic layer deposition. *J. Electrochem. Soc.* **2013**, *160*, F1225–F1231.

70. Onn, T.M.; Zhang, S.; Arroyo-Ramirez, L.; Chung, Y.-C.; Graham, G.W.; Pan, X.; Gorte, R.J. Improved thermal stability and methane-oxidation activity of Pd/Al_2O_3 catalysts by atomic layer deposition of ZrO_2. *ACS Catal.* **2015**, *5*, 5696–5701. [CrossRef]
71. Onn, T.M.; Monai, M.; Dai, S.; Arroyo-Ramirez, L.; Zhang, S.; Pan, X.; Graham, G.W.; Fornasiero, P.; Gorte, R.J. High-surface-area, iron-oxide films prepared by atomic layer deposition on γ-Al_2O_3. *Appl. Catal. A Gen.* **2017**, *534*, 70–77. [CrossRef]
72. Onn, T.M.; Zhang, S.; Arroyo-Ramirez, L.; Xia, Y.; Wang, C.; Pan, X.; Graham, G.W.; Gorte, R.J. High-surface-area ceria prepared by ALD on Al_2O_3 support. *Appl. Catal. B Environ.* **2017**, *201*, 430–437. [CrossRef]
73. Onn, T.M.; Dai, S.; Chen, J.; Pan, X.; Graham, G.W.; Gorte, R.J. High-surface area ceria–zirconia films prepared by atomic layer deposition. *Catal. Lett.* **2017**, *147*, 1464–1470. [CrossRef]
74. Wang, C.; Hu, L.; Lin, Y.; Poeppelmeier, K.; Stair, P.; Marks, L. Controllable ALD synthesis of platinum nanoparticles by tuning different synthesis parameters. *J. Phys. D Appl. Phys.* **2017**, *50*, 415301. [CrossRef]
75. Ramachandran, R.K.; Filez, M.; Dendooven, J.; Galvita, V.V.; Poelman, H.; Solano, E.; Fonda, E.; Marin, G.B.; Detavernier, C. Size- and composition-controlled Pt–Sn bimetallic nanoparticles prepared by atomic layer deposition. *RSC Adv.* **2017**, *7*, 20201–20205. [CrossRef]
76. Berland, B.; Gartland, I.; Ott, A.; George, S.M. In situ monitoring of atomic layer controlled pore reduction in alumina tubular membranes using sequential surface reactions. *Chem. Mater.* **1998**, *10*, 3941–3950. [CrossRef]
77. King, D.M.; Spencer, J.A.; Liang, X.; Hakim, L.F.; Weimer, A.W. Atomic layer deposition on particles using a fluidized bed reactor with in situ mass spectrometry. *Surf. Coat. Technol.* **2007**, *201*, 9163–9171. [CrossRef]
78. De Martin, L.; Bouwman, W.G.; van Ommen, J.R. Multidimensional nature of fluidized nanoparticle agglomerates. *Langmuir* **2014**, *30*, 12696–12702. [CrossRef] [PubMed]
79. De Martín, L.; Fabre, A.; van Ommen, J.R. The fractal scaling of fluidized nanoparticle agglomerates. *Chem. Eng. Sci.* **2014**, *112*, 79–86. [CrossRef]
80. Feng, H.; Libera, J.A.; Stair, P.C.; Miller, J.T.; Elam, J.W. Subnanometer palladium particles synthesized by atomic layer deposition. *ACS Catal.* **2011**, *1*, 665–673. [CrossRef]
81. Najafabadi, A.T.; Khodadadi, A.A.; Parnian, M.J.; Mortazavi, Y. Atomic layer deposited Co/γ-Al_2O_3 catalyst with enhanced cobalt dispersion and Fischer–Tropsch synthesis activity and selectivity. *Appl. Catal. A Gen.* **2016**, *511*, 31–46. [CrossRef]
82. Cheng, N.; Sun, X. Single atom catalyst by atomic layer deposition technique. *Chin. J. Catal.* **2017**, *38*, 1508–1514. [CrossRef]
83. Gould, T.D.; Lubers, A.M.; Neltner, B.T.; Carrier, J.V.; Weimer, A.W.; Falconer, J.L.; Medlin, J.W. Synthesis of supported Ni catalysts by atomic layer deposition. *J. Catal.* **2013**, *303*, 9–15. [CrossRef]
84. He, B.J.-J.; Wang, C.-X.; Zheng, T.-T.; Zhao, Y.-K. Thermally induced deactivation and the corresponding strategies for improving durability in automotive three-way catalysts. *Johns. Matthey Technol. Rev.* **2016**, *60*, 196–203. [CrossRef]
85. Onn, T.M.; Mao, X.; Lin, C.; Wang, C.; Gorte, R.J. Investigation of the thermodynamic properties of surface ceria and ceria–zirconia solid solution films prepared by atomic layer deposition on Al_2O_3. *Inorganics* **2017**, *5*, 69.
86. Senthilkumar, B.; Selvan, R.K.; Meyrick, D.; Minakshi, M. Synthesis and Characterization of Manganese Molybdate for Symmetric Capacitor Applications. *Int. J. Electrochem. Sci.* **2015**, *10*, 185–193.
87. Barmi, M.J.; Minakshi, M. Tuning the Redox Properties of the Nanostructured $CoMoO_4$Electrode: Effects of Surfactant Content and Synthesis Temperature. *ChemCatChem* **2016**, *81*, 964–977.
88. Héroguel, F.; Le Monnier, B.P.; Brown, K.S.; Siu, J.C.; Luterbacher, J.S. Catalyst stabilization by stoichiometrically limited layer-by-layer overcoating in liquid media. *Appl. Catal. B Environ.* **2017**, *218*, 643–649. [CrossRef]
89. Lu, J.; Liu, B.; Greeley, J.P.; Feng, Z.; Libera, J.A.; Lei, Y.; Bedzyk, M.J.; Stair, P.C.; Elam, J.W. Porous alumina protective coatings on palladium nanoparticles by self-poisoned atomic layer deposition. *Chem. Mater.* **2012**, *24*, 2047–2055. [CrossRef]
90. Lu, J.; Elam, J.W.; Stair, P.C. Synthesis and stabilization of supported metal catalysts by atomic layer deposition. *Acc. Chem. Res.* **2013**, *46*, 1806–1815. [CrossRef] [PubMed]

91. Lee, J.; Jackson, D.H.; Li, T.; Winans, R.E.; Dumesic, J.A.; Kuech, T.F.; Huber, G.W. Enhanced stability of cobalt catalysts by atomic layer deposition for aqueous-phase reactions. *Energy Environ. Sci.* **2014**, *7*, 1657–1660. [CrossRef]
92. Lu, J.; Fu, B.; Kung, M.C.; Xiao, G.; Elam, J.W.; Kung, H.H.; Stair, P.C. Coking- and sintering-resistant palladium catalysts achieved through atomic layer deposition. *Science* **2012**, *335*, 1205–1208. [CrossRef] [PubMed]
93. Kim, Y.B.; Holme, T.P.; Gür, T.M.; Prinz, F.B. Surface-modified low-temperature solid oxide fuel cell. *Adv. Funct. Mater.* **2011**, *21*, 4684–4690. [CrossRef]
94. Nieminen, M.; Lehto, S.; Niinistö, L. Atomic layer epitaxy growth of $LaGaO_3$ thin films. *J. Mater. Chem.* **2001**, *11*, 3148–3153. [CrossRef]
95. Gourba, E.; Ringuede, A.; Cassir, M.; Billard, A.; Päiväsaari, J.; Niinistö, J.; Putkonen, M.; Niinistö, L. Characterisation of thin films of ceria-based electrolytes for intermediatetemperature—Solid oxide fuel cells (IT-SOFC). *Ionics* **2003**, *9*, 15–20. [CrossRef]
96. Fan, Z.; Chao, C.-C.; Hossein-Babaei, F.; Prinz, F.B. Improving solid oxide fuel cells with yttria-doped ceria interlayers by atomic layer deposition. *J. Mater. Chem.* **2011**, *21*, 10903–10906. [CrossRef]
97. Chang, I.; Ji, S.; Park, J.; Lee, M.H.; Cha, S.W. Ultrathin YSZ coating on Pt cathode for high thermal stability and enhanced oxygen reduction reaction activity. *Adv. Energy Mater.* **2015**, *5*, 1402251. [CrossRef]
98. Jiang, X.; Huang, H.; Prinz, F.B.; Bent, S.F. Application of atomic layer deposition of platinum to solid oxide fuel cells. *Chem. Mater.* **2008**, *20*, 3897–3905. [CrossRef]
99. Holme, T.P.; Lee, C.; Prinz, F.B. Atomic layer deposition of LSM cathodes for solid oxide fuel cells. *Solid State Ion.* **2008**, *179*, 1540–1544. [CrossRef]
100. Lie, M.; Nilsen, O.; Fjellvåg, H.; Kjekshus, A. Growth of $La_{1-x}Sr_xFeO_3$ thin films by atomic layer deposition. *Dalton Trans.* **2009**, *3*, 481–489. [CrossRef] [PubMed]
101. Kenjo, T.; Osawa, S.; Fujikawa, K. High temperature air cathodes containing ion conductive oxides. *J. Electrochem. Soc.* **1991**, *138*, 349–355. [CrossRef]
102. Østergård, M.; Clausen, C.; Bagger, C.; Mogensen, M. Manganite-zirconia composite cathodes for SOFC: Influence of structure and composition, *Electrochim. Acta* **1995**, *40*, 1971–1981. [CrossRef]
103. Gong, Y.; Palacio, D.; Song, X.; Patel, R.L.; Liang, X.; Zhao, X.; Goodenough, J.B.; Huang, K. Stabilizing nanostructured solid oxide fuel cell cathode with atomic layer deposition. *Nanoletters* **2013**, *13*, 4340–4345. [CrossRef] [PubMed]
104. Choi, H.J.; Bae, K.; Jang, D.Y.; Kim, J.W.; Shim, J.H. Performance degradation of lanthanum strontium cobaltite after surface modification. *J. Electrochem. Soc.* **2015**, *162*, F622–F626. [CrossRef]
105. Sbrockey, N.; Aindow, M.; Deljoo, B.; Ghezel-Ayagh, H.; Torabi, A.; Tompa, G. Fluidized bed production of surface functionalized powders for solid oxide fuel cell cathodes. *ECS Trans.* **2017**, *78*, 817–825. [CrossRef]
106. Karimaghaloo, A.; Andrade, A.M.; Grewal, S.; Shim, J.H.; Lee, M.H. Mechanism of cathodic performance enhancement by a few-nanometer-thick oxide overcoat on porous Pt cathodes of solid oxide fuel cells. *ACS Omega* **2017**, *2*, 806–813. [CrossRef]
107. Liu, K.-Y.; Fan, L.; Yu, C.-C.; Su, P.-C. Thermal stability and performance enhancement of nano-porous platinum cathode in solid oxide fuel cells by nanoscale ZrO_2 capping. *Electrochem. Commun.* **2015**, *56*, 65–69. [CrossRef]
108. Koide, H.; Someya, Y.; Yoshida, T.; Maruyama, T. Properties of Ni/YSZ cermet as anode for SOFC. *Solid State Ion.* **2000**, *132*, 253–260. [CrossRef]
109. Malzbender, J.; Wessel, E.; Steinbrech, R.W. Reduction and re-oxidation of anodes for solid oxide fuel cells. *Solid State Ion.* **2005**, *176*, 2201–2203. [CrossRef]
110. Klemensø, T.; Chung, C.; Larsen, P.H.; Mogensen, M. The mechanism behind redox instability of anodes in high-temperature SOFCs. *J. Electrochem. Soc.* **2005**, *152*, A2186–A2192. [CrossRef]
111. Noh, H.-S.; Son, J.-W.; Lee, H.; Ji, H.-I.; Lee, J.-H.; Lee, H.-W. Suppression of Ni agglomeration in PLD fabricated Ni-YSZ composite for surface modification of SOFC anode. *J. Eur. Ceram. Soc.* **2010**, *30*, 3415–3423. [CrossRef]
112. Matsui, T.; Eguchi, K.; Shirai, K.; Ozeki, T.; Okanishi, T.; Muroyama, H.; Eguchi, K. Redox-induced self-modification of cermet anodes of Ni–CeO_2-based oxide for solid oxide fuel cells. *J. Electrochem. Soc.* **2017**, *164*, F1368–F1374. [CrossRef]